Progress In Electromagnetics Research, Vol. 130, 601–617, 2012

DETERMINATION OF DIELECTRIC PROPERTY OF CONSTRUCTION MATERIAL PRODUCTS USING A NOVEL RFID SENSOR

R. Suwalak[1], C. Phongcharoenpanich[1, *], D. Torrungrueng[2], and M. Krairiksh[1]

[1]Faculty of Engineering, King Mongkut's Institute of Technology Ladkrabang, Bangkok 10520, Thailand

[2]Faculty of Engineering and Technology, Asian University, Banglamung, Chonburi 20260, Thailand

Abstract—This paper presents a concept, by which radio frequency (RF) tags are employed as remotely read dielectric-property sensors to determine qualities of some construction material products (CMPs); e.g., light weight concrete (LWC), mortar specimens and concrete. Using the dependency of the read range of the passive RF identification (RFID) sensor system on the electromagnetic properties of CMPs near or in contact with RFID tags, the qualities of CMPs can be determined through their estimated dielectric properties. Theoretical formulation is provided, and numerical simulations are performed for optimal design of passive RFID tag antennas suitable for RFID sensors and for read-range calculations. In addition, a series of measurements is performed to measure read ranges of the passive RFID sensor system for an LWC as an example of CMPs, and these measured read ranges will be processed appropriately to inversely determine the dielectric constant of the LWC under test, which in turn provides information on its qualities. It is found that the novel RFID sensor can be employed to determine the dielectric properties of the LWC under test with reasonable accuracy.

1. INTRODUCTION

The demand for traceability to identify and inspect qualities of material products through nondestructive testing (NDT) techniques has been on the rise. Several NDT techniques, such as radar, capacimetry, electrical

Received 1 July 2012, Accepted 27 August 2012, Scheduled 3 September 2012

* Corresponding author: Chuwong Phongcharoenpanich (kpchuwon@kmitl.ac.th).

resistance and ultrasonic waves, have been extensively used [1–6]. Each technique however has its advantages and disadvantages, so the selection of an appropriate technique is based on the desired application. For such construction materials (CMs) as light weight concrete (LWC), mortar specimens and concrete, a reliable NDT technique is required to evaluate their properties whether they are suitable for construction use. Therefore, the development of a reliable sensor technique to determine material quality in manufacturing and/or material testing and inspection process is necessary.

For the ultra high frequency (UHF) and microwave frequency radio-frequency identification (RFID) systems [7], passive modulated backscatter RF tags communicate with a reader, using far-field electromagnetic (EM) waves, and these tags typically modulate the EM waves scattered from tag antennas using the load modulation [7]. To maximize the tag performance, tag antennas must be appropriately designed to conjugately match the chip impedance [8].

One important factor of tag performance is the read range of the passive RFID system, defined as the maximum distance from which a tag can be detected. One limitation on the read range is the maximum distance from which the tag receives merely sufficient power to turn on and scatter back. Another limitation is the maximum distance from which the reader can detect this scattered signal. The read range is the smaller of the two maximum distances. Typically, the former determines the read range since the RFID reader sensitivity is usually high [9]. From the sensor's viewpoint, the dependency of the read range on EM properties of CMs near or in contact with tags can be employed as an approach to determining quality of CMs through their estimated dielectric constants.

RF tag performance is affected by many factors, including EM properties of objects near or in contact with tags [10, 11]. In addition, Siden et al. presented a concept by which pairs of ordinary RFID tags are exploited as remotely read moisture sensors [12]. The moisture sensing label incorporating two RFID tags is embedded in a wall, under which one of the tags is covered with a moisture absorbent material while the other is a naked tag. They are used to detect leaking water pipe connections hidden behind the walls. Additionally, the attenuation and equivalent electric parameters of brick and reinforced concrete walls are estimated [13]. Furthermore, Marrocco et al. have presented the development of very low-cost passive RFID devices capable of monitoring the features of moving objects without the need for specific sensors. Instead, the multiport tag antennas are used as a sensor since they exploit the dependency of the tag's input impedances and the radar cross section on the physical and geometrical features of

a real target [14]. However, the purpose of this paper is to describe the possible classification and detection performances of multiport sensor tags in a unitary context.

In this paper, an NDT technique, called a novel RFID sensor, operating in the UHF band is proposed to determine quality of certain CMs through their estimated dielectric properties. Generally, the traditional RFID sensors require additional specific sensors, such as humidity, temperature, motion, light and sound sensors, to be integrated with RFID tags [15–17]. On the other hand, the novel RFID sensor does not require additional specific sensors to determine dielectric properties of the materials under test, thereby more convenient in fabrication and usually of lower cost. In addition, the novel RFID sensor does not require a network analyzer and other expensive accessories. The key component of the novel RFID sensor is the tag specifically designed to achieve the conjugate impedance matching condition between the tag antenna and a chip in the presence of a selected member of the family of materials of interest, which is near or in contact with the tag. Typically, two specifically designed tags (SDTs), to subsequently discuss in greater detail, for selected members of the family are required to uniquely determine the dielectric properties of a lossy CM of interest.

The organization of this paper is as follows. The introduction is in Section 1. Section 2 presents the associated theory and relevant formulas for the novel RFID sensor. Simulation and measurement results are illustrated in Section 3, where the $e^{j\omega t}$ harmonic time convention is assumed, ω is the angular frequency and $j = \sqrt{-1}$ is a complex constant. Conclusions are discussed in Section 4.

2. THEORY

Figure 1 illustrates a novel RFID sensor system consisting of the RFID reader, the reader antenna and SDTs, where each SDT is placed near or in contact with a material product under test. Note that the read range is normally governed by the maximum distance from which a tag

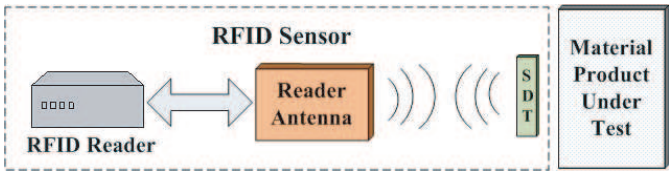

Figure 1. A novel RFID sensor system.

receives just sufficient power to turn on and scatter back due to the fact that the RFID reader sensitivity is usually high. Using the modified Friis transmission equation [18, 19], the maximum distance ($R_{\max,mat}$) of tags in the presence of material products near or in contact with tags can be calculated, under the assumption that the reader antenna has perfect impedance matching and perfect polarization matching to the tag antenna. In addition, Griffin et al. proposed new forms of the power and backscatter communication radio link budgets in terms of the gain penalty based on the modified Friis transmission equation, which is the decrease in tag antenna gain from its free space value when attached to a material, and these forms allow RF tag designers to quantify the effects of tag material attachment [20, 21], as follows:

$$R_{\max,mat} = \frac{\lambda}{4\pi}\sqrt{\frac{P_{reader\text{-}tx} \cdot G_{reader\text{-}tx} \cdot \tau_{mat}}{L_{sys} \cdot P_{tag,th}} \cdot \left(\frac{G_{tag,fs}}{GP}\right)}, \quad (1)$$

where $P_{reader\text{-}tx}$ is the input power to the reader antenna, L_{sys} the system loss in both tag and reader, $G_{reader\text{-}tx}$ the gain of the reader antenna, $P_{tag,th}$ the minimum threshold power necessary to power up the chip, $G_{tag,fs}$ is tag antenna gain in free space, λ is free space wavelength, GP is the gain penalty due to the presence of a material product, and τ_{mat} the power transmission coefficient in the presence of a material product. In general, the power transmission coefficient τ can be expressed in terms of the power-wave reflection coefficient Γ_p at the tag antenna terminal as [8, 22]

$$\tau = 1 - |\Gamma_p|^2, \quad (2)$$

where

$$\Gamma_p \equiv \frac{Z_{chip} - Z^*_{ant,tag}}{Z_{chip} + Z_{ant,tag}}. \quad (3)$$

In (3), the superscript "*" denotes the complex conjugate symbol, and Z_{chip} and $Z_{ant,tag}$ are the chip impedance and the tag antenna impedance, respectively. Note that when the chip impedance and the tag antenna impedance are conjugately matched ($Z_{chip} = Z^*_{ant,tag}$), Γ_p is equal to zero and τ is equal to one as expected.

Similarly, the maximum distance ($R_{\max,fs}$) of tags in free space can be calculated under the same assumption as $R_{\max,mat}$ as follows:

$$R_{\max,fs} = \frac{\lambda}{4\pi}\sqrt{\frac{P_{reader\text{-}tx} \cdot G_{reader\text{-}tx} \cdot \tau_{fs} \cdot G_{tag,fs}}{L_{sys} \cdot P_{tag,th}}} \quad (4)$$

where τ_{fs} is the power transmission coefficient associated with the tag antenna in free space. It should be pointed out that the term GP in (4)

is equal to 1 since tags are in the free space. From (1) and (4), the ratio of $R_{\max,mat}$ to $R_{\max,fs}$ can be expressed compactly as

$$\frac{R_{\max,mat}}{R_{\max,fs}} = \sqrt{\frac{\tau_{mat}}{\tau_{fs}}\left(\frac{1}{GP}\right)} \tag{5}$$

where all common terms in (1) and (4) are cancelled out and only terms associated with the power transmission coefficients and the tag antenna gains remain. In (5), only terms τ_{mat} and GP are dependent on properties of material products near or in contact with tags; e.g., their dielectric constants, sizes and shapes, in a complicated fashion. Thus, the ratio $R_{\max,mat}/R_{\max,fs}$ can usually be obtained via measurements or numerical simulations of associated problems. Note that all parameters on the right-hand side of (5) are related to two parameters of tag antennas; i.e., the tag antenna impedance and the tag antenna gain, in free space and in the presence of a material product. Once the ratio $R_{\max,mat}/R_{\max,fs}$ is known, the dielectric constant of the material product of interest can be estimated to determine their qualities using appropriate data processing. The procedure of dielectric constant determination will be illustrated via specific examples in the next section.

3. SIMULATION AND MEASUREMENT RESULTS

Figure 2 shows the novel RFID sensor setup in an anechoic chamber, where the operating frequency of interest is 922.5 MHz. The proposed RFID sensor employs the UHF RFID reader of Symbol XR450 and the reader antenna using the Anritsu antenna with the model of MP651A as a half-wavelength standard tuned dipole antenna [23]. Owing to the fact that the standard dipole has the linear polarization and tag

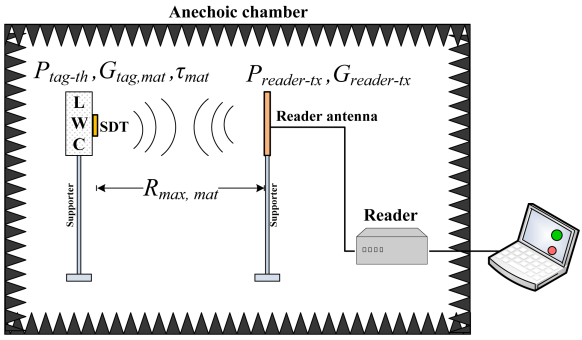

Figure 2. The novel RFID sensor setup.

Table 1. Dielectric constant of lossy LWCs.

LWC state	ε_r'	ε_r''
Dry	2.5	0.2
Saturated	8	1.08

antennas are designed to achieve the same polarization as the standard dipole, there is no polarization mismatch. In addition, due to the fact that the RFID reader sensitivity is high, the read range is equal to the maximum distance from tag calculated by using the modified Friis transmission equation as shown in (1). In this study, all tags are designed via the CST Microwave Studio simulator [24] and using the IC chip NXP UCODE G2XL, where its input impedance is equal to $16.5 - j148.7\,\Omega$ at 922.5 MHz [25]. In Figure 2, the LWC is employed as an example of CMPs to illustrate the concept of the novel RFID sensor. Note that the LWC is assumed to be homogeneous and it can usually be used to construct buildings due to its light weight, easily sawn and sculpted, and nailed or screwed without pre-drilling [26].

Typically, the actual dimension for commercial application of LWC is 20 cm × 60 cm × 7.5 cm [27]. Its sample with the dimension of 20 cm × 15 cm × 7.5 cm is considered in this paper. The following parameters are employed: $P_{reader\text{-}tx} = 20\,\text{dBm}$, $L_{sys} = 1.01\,\text{dB}$, $G_{reader\text{-}tx} = 2.15\,\text{dBi}$ and $P_{tag,th} = -15\,\text{dBm}$. All SDTs are fabricated on the 0.8 mm-FR4 substrate with the dielectric constant of 4.3. Two cases are considered; i.e., lossless and lossy LWCs. The former will be considered first since it is simpler to understand the methodology of the proposed RFID sensor, while the latter is more complicated, but more realistic.

For the lossy case, two LWC states are considered; i.e., the dry state and the saturated state with water. In literature, the constitutive parameters of building materials were measured [28–32]. Note that the dielectric constant of the lossy case can be measured using the dielectric probe [33]. Table 1 illustrates the dielectric constants, ε_r, of each lossy LWC state, where ε_r is defined as $\varepsilon_r = \varepsilon_r' - j\varepsilon_r''$. As expected, ε_r' and ε_r'' of the saturated state are larger than ε_r' and ε_r'' of the dry state respectively, due to the water existing in the saturated state.

3.1. Lossless LWC

For the lossless LWC case, it is assumed that its dielectric constant is equal to the dielectric constant of LWC in the dry state with no loss; i.e., $\varepsilon_r = \varepsilon_r' = 2.5$ and $\varepsilon_r'' = 0$. Using the CST Microwave

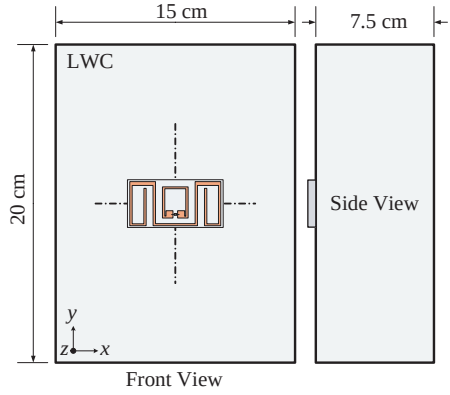

Figure 3. The SDT location on the LWC.

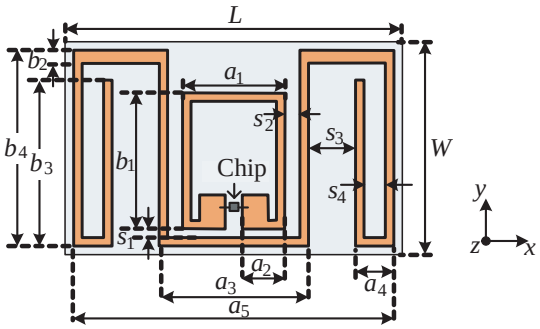

Figure 4. The SDT for the lossless LWC.

Studio simulator, the tag antenna of the SDT, called the SDT_{LL}, is appropriately designed to conjugately match with the chip impedance by including effects of the lossless LWC in the simulation, where the SDT_{LL} is attached to the surface of the lossless LWC at its center as shown in Figure 3 to reduce edge effects. Symmetrical meander line antennas are employed in this paper with an inductively coupled structure with 1-mm line thickness [34] to flexibly meet the high Q-factor of the IC chip NXP UCODE G2XL. In addition, the tag antenna size must be compact to mount on small LWCs as well. The tag antenna structure is optimized as shown in Figure 4, where its antenna parameters are illustrated in Table 2.

Note that the dimensions of the SDT_{LL} are equal to 39.5 mm $\times$ 25 mm $\times$ 0.8 mm after optimization, where its input impedance is equal to $17.75 + j147.8\,\Omega$, and its polarization in the bore-sight direction

Table 2. Parameters of the SDT_{LL} for the lossless LWC with $\varepsilon_r = 2.5$.

Parameter	Dimension (mm)	Parameter	Dimension (mm)
a_1	12	b_4	23
a_2	5	L	39.5
a_3	17.5	s_1	1
a_4	5	s_2	1.75
a_5	38.5	s_3	5
b_1	16.5	s_4	3
b_2	1.5	W	25
b_3	18.5		

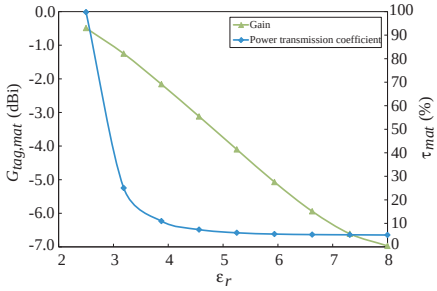

Figure 5. $G_{tag,mat}$ and τ_{mat} as a function of ε_r for the SDT_{LL}.

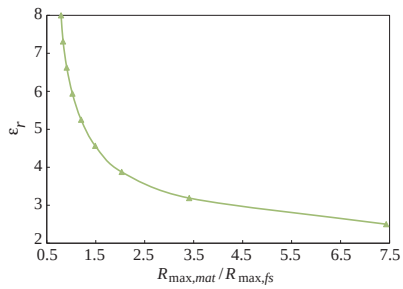

Figure 6. The relation between ε_r and $R_{\text{max},mat}/R_{\text{max},fs}$ for the SDT_{LL} obtained from the simulations.

looking out from the LWC is horizontal. In addition, its gain and power transmission coefficient ($G_{tag,mat}$ and τ_{mat}) are found to be -0.49 dBi and 99.8%, respectively. Note that τ_{mat} of the SDT_{LL} is almost equal to 100% illustrating that the input impedances of the SDT_{LL} and the IC chip are almost conjugately matched as desired.

To show the dependency of $G_{tag,mat}$ and τ_{mat} on ε_r, Figure 5 illustrates the plots of $G_{tag,mat}$ in dBi and τ_{mat} in percentage for the SDT_{LL} as a function of ε_r ranging from 2.5 to 8.0. It is found that its $G_{tag,mat}$ and τ_{mat} monotonically decrease as ε_r increases, where both $G_{tag,mat}$ and τ_{mat} are maximum at $\varepsilon_r = 2.5$. Due to the fact that the SDT_{LL} is specifically designed to conjugately match with the chip impedance in the presence of the lossless LWC with $\varepsilon_r = 2.5$, more impedance mismatch occurs as increasing ε_r, resulting in decreasing τ_{mat} as expected.

For this case, only ε_r' of the lossless LWC under test is required ($\varepsilon_r'' = 0$). It will be shown that only one SDT is sufficient to

uniquely determine ε'_r from the measurements of associated read ranges. Figure 6 illustrates the plot of $\varepsilon_r = \varepsilon'_r$ versus $R_{\max,mat}/R_{\max,fs}$ for the $\mathrm{SDT_{LL}}$, obtained from the simulation by using (5), where $R_{\max,fs}$ is a normalization constant. As expected from Figures 5 and 6, $R_{\max,mat}/R_{\max,fs}$ monotonically decreases as ε_r increases. It is clear from Figure 6 that once $R_{\max,mat}/R_{\max,fs}$ of the $\mathrm{SDT_{LL}}$ attached to the lossless LWC under test is known from the measurements, its ε_r can be uniquely estimated using Figure 6.

3.2. Lossy LWC

For the lossy LWC case, the tags are specifically designed for optimum performance for each state of lossy LWCs as shown in Table 1. The RFID tag structures optimized for the dry LWC state, called the $\mathrm{SDT_1}$, and for the saturated LWC state, called the $\mathrm{SDT_2}$. They are illustrated

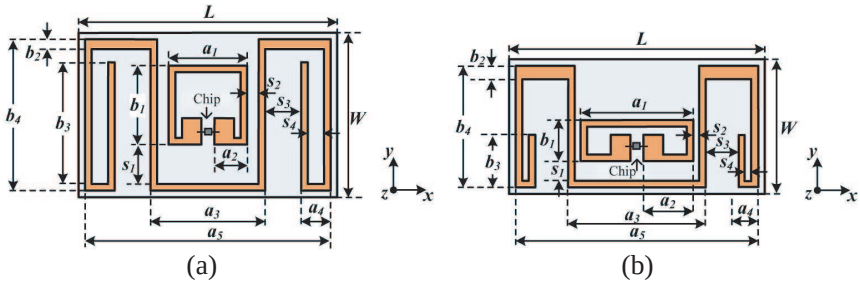

Figure 7. The SDTs for the lossy LWCs. (a) Dry LWC SDT ($\mathrm{SDT_1}$). (b) Saturated LWC SDT ($\mathrm{SDT_2}$).

Table 3. Tag parameters for the lossy LWCs.

Parameter	Dimension (mm)		Parameter	Dimension (mm)	
	$\mathrm{SDT_1}$	$\mathrm{SDT_2}$		$\mathrm{SDT_1}$	$\mathrm{SDT_2}$
a_1	12	17	b_4	23	18.5
a_2	5	7.5	L	39.5	39
a_3	17.5	21	s_1	6	3
a_4	4.5	3	s_2	1.75	1
a_5	37.5	37	s_3	5.5	5
b_1	12	6	s_4	2.5	1
b_2	1.5	2	W	25	20.5
b_3	19.5	8			

in Figures 7(a) and 7(b) respectively, where their parameters are shown in Table 3. The dimensions of the SDT_1 and the SDT_2 are equal to 39.5 mm × 25 mm × 0.8 mm and 39 mm × 20.5 mm × 0.8 mm respectively, where their characteristics are tabulated in Table 4. It should be pointed out that τ_{mat} of both SDT_1 and SDT_2 are nearly equal to 100% as desired.

To illustrate the dependency of $G_{tag,mat}$ and τ_{mat} on ε_r' for two specific values of ε_r'', let first consider $\varepsilon_r'' = 0.2$ as shown in Figure 8, where the SDT_1, specifically designed for $\varepsilon_r = 2.5 - j0.2$, is employed in this study. Like the lossless case, it is found that τ_{mat} tends to decrease as ε_r' increases as expected due to more impedance mismatch. In addition, $G_{tag,mat}$ varies noticeably as ε_r' increases. Next, let consider another case of $\varepsilon_r'' = 1.08$ as shown in Figure 9, where the SDT_2, specifically designed for $\varepsilon_r = 8.0 - j1.08$, is employed. Note that τ_{mat} tends to increase as ε_r' increases as expected due to less impedance mismatch, and $G_{tag,mat}$ tends to increase and then decrease as ε_r' increases. It can be concluded from these two cases that an SDT, specifically designed for an LWC with $\varepsilon_r' = \tilde{\varepsilon}_r' - j\tilde{\varepsilon}_r''$, usually possesses the maximum τ_{mat} when $\varepsilon_r' = \tilde{\varepsilon}_r'$ and $\varepsilon_r'' = \tilde{\varepsilon}_r''$. However, the associated $G_{tag,mat}$ is not always the maximum.

Table 4. SDT characteristics for the lossy LWCs.

SDT Characteristic	SDT_1	SDT_2
Input impedance (Ω)	$14.09 + j149.41$	$16.09 + j147.64$
$G_{tag,mat}$ (dBi)	−8.66	−10.67
τ_{mat} (%)	99.33	98.88
Polarization	Linear	Linear

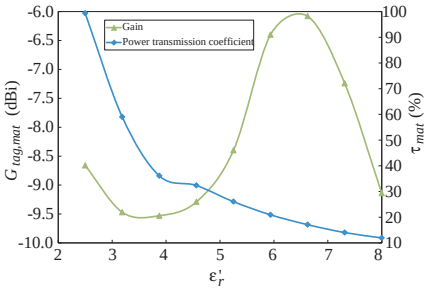

Figure 8. $G_{tag,mat}$ and τ_{mat} as a function of ε_r' for the SDT_1 with $\varepsilon_r'' = 0.2$.

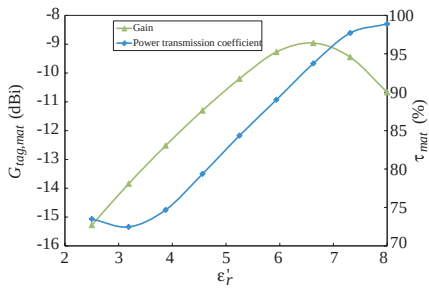

Figure 9. $G_{tag,mat}$ and τ_{mat} as a function of ε_r' for the SDT_2 with $\varepsilon_r'' = 1.08$.

3.3. Measurements

The read range between the RFID reader and SDTs are measured in an anechoic chamber as illustrated in Figure 10. The prototypes of

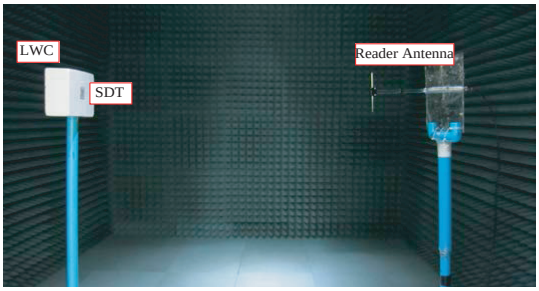

Figure 10. The RFID sensor measurement setup in an anechoic chamber.

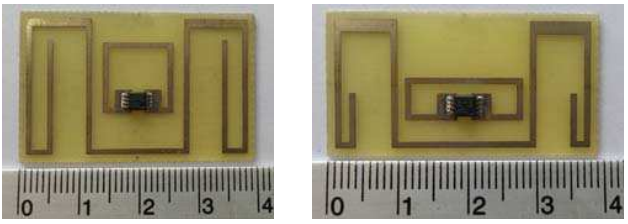

(a) (b)

Figure 11. The SDT prototypes. (a) SDT_1 for the dry LWC. (b) SDT_2 for the saturated LWC.

Figure 12. The photograph of an SDT attached to the LWC of interest.

Table 5. Read range of SDTs attached to lossy LWCs under test.

LWC State	Simulation (cm)	Measurement (cm)
Dry	68.3	69
Saturated	54.7	50

the SDT_1 and the SDT_2 are a printed meander line with a coupling loop on the FR4 substrate as shown in Figure 11. An SDT attached to the LWC of interest is shown in Figure 12. From measurements, the read ranges of SDTs attached to lossy LWCs under test are shown in Table 5. The read ranges from the simulations and measurements agree reasonably well. The discrepancies between the simulated and measured results may derive from the measurement error and the SDT fabrication error. Therefore, the measured read range can be used to inversely determine the dielectric constant of LWCs under test with reasonable accuracy.

3.4. Dielectric-constant Determination Procedure

Once the read ranges of all SDTs attached to the LWC under test are known via measurements, including the corresponding read ranges of the SDTs in the free space, the dielectric constant of the LWC under test can be determined from the following procedure.

For the lossy LWC case, both ε_r' and ε_r'' of the lossy LWC under test are required. It will be shown that two SDTs are required to uniquely determine both ε_r' and ε_r'' from the measurements of associated read ranges. In this study, the SDT_1 and the SDT_2, specifically designed for the dry and saturated LWC states respectively, are attached to the lossy LWC under test. Using the simulations, the plot of ε_r' versus $R_{\max,mat}/R_{\max,fs}$ for each SDT is illustrated in Figure 13 for $\varepsilon_r'' = 0.20$, 0.64 and 1.08. It is clearly seen from Figure 13 that either SDT_1 or SDT_2 alone cannot be employed to uniquely determine ε_r' and ε_r'' from a measurement of $R_{\max,mat}/R_{\max,fs}$ since several combinations of ε_r' and ε_r'' yield the same $R_{\max,mat}/R_{\max,fs}$. However, using both SDT_1 and SDT_2 with a measurement of $R_{\max,mat}/R_{\max,fs}$ for each SDT, ε_r' and ε_r'' can be determined uniquely as shown in the following two examples.

Consider a sample of lossy LWCs (sample#1) as shown in Figure 13(a), where its dielectric constant ε_r is equal to $7.5 - j1.08$ obtained from the dielectric probe measurement [33], which requires a network analyzer. From the read range measurements, it is found that $R_{\max,mat}/R_{\max,fs}$ for the SDT_1 and the SDT_2 are equal to 0.5 and 2.10 respectively, as shown in Figure 13(a) as the two vertical

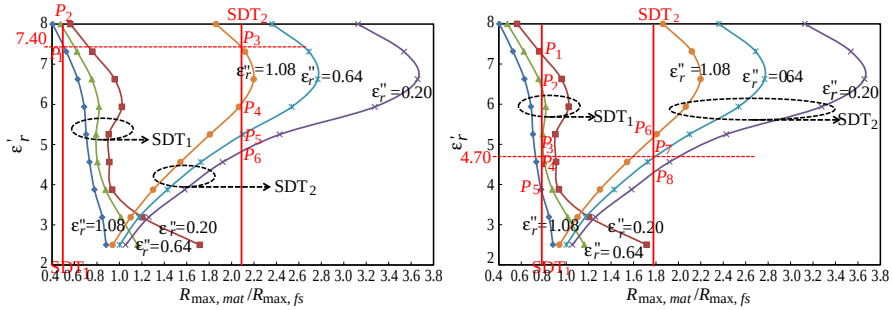

Figure 13. The relation between ε'_r and $R_{\max,mat}/R_{\max,fs}$ for the SDT_1 and the SDT_2 with $\varepsilon''_r = 0.20$, 0.64 and 1.08 obtained from the simulations. (a) The LWC sample#1. (b) The LWC sample#2.

lines. It should be pointed out that the maximum distances $R_{\max,fs}$ of each SDT are generally different. In Figure 13(a), each vertical line of $R_{\max,mat}/R_{\max,fs}$ intersects the family of the $\varepsilon'_r - R_{\max,mat}/R_{\max,fs}$ curves for each SDT at P_1 and P_2 for the SDT_1 and P_3, P_4, P_5 and P_6 for the SDT_2. At each intersection point, a pair of ε'_r and ε''_r is obtained. Due to the fact that the sample of lossy LWCs is identical for both SDT_1 and SDT_2, only the intersection points, providing the identical pair of ε'_r and ε''_r, are valid. It can be seen from Figure 13(a) that the intersection points P_1 and P_3 correspond to $(\varepsilon'_r, \varepsilon''_r) = (7.40, 1.08)$, which is the estimated dielectric constant of the LWC sample#1.

Consider another sample of lossy LWCs (sample#2), where its dielectric constant ε_r is equal to $4.8 - j0.4$ obtained from the dielectric probe measurement [33]. Using the same determination procedure as in the case of the LWC sample#1, $R_{\max,mat}/R_{\max,fs}$ for the SDT_1 and the SDT_2 are found to be 0.77 and 1.77 respectively, as shown in Figure 13(b) as the two vertical lines. It can be seen from this Figure that the intersection points P_4 and P_7 correspond to $(\varepsilon'_r, \varepsilon''_r) = (4.70, 0.64)$, which is the estimated dielectric constant of the LWC sample#2. Thus, two SDTs can be employed to uniquely determine the dielectric constant of the lossy LWC under test. For these examples, the relative error of 1.3% and 5.4% for sample#1 and sample#2, respectively, can be obtained using the novel RFID sensor, which is reasonably accurate. It should be pointed out that the relative error can be decreased by reducing the measurement error of associated read ranges and the SDT fabrication error. Once the dielectric constant of the LWC sample is estimated, the quality of the LWC sample can be determined by using the relation between the dielectric constant and the LWC quality, predetermined by measurements and testings or other approaches [35–37].

4. CONCLUSIONS

A novel RFID sensor technique operating in the UHF band is proposed to determine quality of certain CMs through their estimated dielectric properties. It is an NDT technique that does not require additional specific sensors to determine dielectric properties of the materials under test, thereby more convenient in fabrication and usually of lower cost. The promising approach based on a novel RFID sensor is successfully employed to determine the dielectric property of LWC samples through associated read-range measurements. The dielectric-constant determination procedures for both lossless and lossy LWCs are discussed in detail in this paper. It is found that the novel RFID sensor provides reasonably accurate results. To use this RFID sensor, it is necessary to know size and shape of material under test, and then perform simulation for desired size and shape first. Future works include reducing associated errors of estimating the dielectric constant of CMPs and other interest materials. In addition, effects of sizes and shapes of materials under test will also be studied based on the same sensor principle, including the sensitivity analysis and practical approaches to mount SDTs on these materials.

ACKNOWLEDGMENT

The authors wish to thank Ms. K. Lertsakwimarn for her assistance in performing associated measurements. This work has been supported by Thailand Graduate Institute of Science and Technology (TGIST), National Science and Technology Development Agency (NSTDA) under contract TGIST 01-51-067, while that of C. Phongcharoenpanich, D. Torrungrueng and M. Krairiksh was funded by the TRF through the Senior Research Scholar Program under Grant No. RTA5180002.

REFERENCES

1. Laurens, S., J. P. Balayssac, J. Rhazi, G. Klysz, and G. Arliguie, "Non-destructive evaluation of concrete moisture by GPR: Experimental study and direct modeling," *RILEM Materials and Structures*, Vol. 38, 827–832, Jan. 2005.
2. Buyukozturk, O., "Electromagnetic properties of concrete and their significance in nondestructive testing," *Transport. Research Board*, Paper No. 970872, 1997.
3. Hasar, U. C., "Thickness-independent complex permittivity determination of partially filled thin dielectric materials into

rectangular waveguides," *Progress In Electromagnetics Research*, Vol. 93, 189–203, 2009.

4. Hasar, U. C., "Thickness-independent automated constitutive parameters extraction of thin solid and liquid materials from waveguide measurements," *Progress In Electromagnetics Research*, Vol. 92, 17–32, 2009.
5. Zhang, H., S. Y. Tan, and H. S. Tan, "An improved method for microwave nondestructive dielectric measurement of layered media," *Progress In Electromagnetics Research B*, Vol. 10, 145–161, 2008.
6. Capineri, L., D. J. Daniels, P. Falorni, O. L. Lopera, and C. G. Windsor, "Estimation of relative permittivity of shallow soils by using the ground penetrating radar response from different buried targets," *Progress In Electromagnetics Research Letters*, Vol. 2, 63–71, 2008.
7. Finkenzeller, K., *RFID Handbook: Radio-frequency Identification Fundamentals and Applications*, Wiley, New York, 1999.
8. Nikitin, P. V., K. V. S. Rao, S. F. Lam, V. Pillai, R. Martinez, and H. Heinrich, "Power reflection coefficient analysis for complex impedances in RFID tag design," *IEEE Trans. Microw. Theory Tech.*, Vol. 53, No. 9, 2721–2725, Sep. 2005.
9. Symbol XR450, [Online] Available: http://www.motorola.com/Business/US-EN/Business+Product+and+Services/RFID/RFID+Rea ders/XR450+Fixed+RFID+Reader_US-En.
10. Marrocco, G., "RFID antennas for the UHF remote monitoring of human subjects," *IEEE Trans. Antennas Propagat.*, Vol. 55, No. 6, 1862–1870, Jun. 2007.
11. Deleruyelle, T., P. Pannier, M. Egels, and E. Bergeret, "An RFID tag antenna tolerant to mounting on materials," *IEEE Antennas Propag. Mag.*, Vol. 52, No. 4, 14–19, Aug. 2010.
12. Siden, J., X. Zeng, T. Unander, A. Koptyug, and H. E. Nilsson, "Remote moisture sensing utilizing ordinary RFID tags," *2007 IEEE Sensors Conference*, 308–311, Oct. 2007.
13. Pena, D., R. Feick, H. D. Hristov, and W. Grote, "Measurement and modeling of propagation losses in brick and concrete walls for the 900-MHz band," *IEEE Trans. Antennas Propagat.*, Vol. 51, No. 1, 31–39, 2003.
14. Marrocco, G., L. Mattioni, and C. Calabrese, "Multiport sensor RFIDs for wireless passive sensing of objects — Basic theory and early results," *IEEE Trans. Antennas Propagat.*, Vol. 56, No. 8, 2691–2702, Aug. 2008.

15. Occhiuzzi, C., S. Cippitelli, and G. Marrocco, "Modeling, design and experimentation of wearable RFID sensor tag," *IEEE Trans. Antennas Propagat.*, Vol. 58, No. 8, 2490–2498, Aug. 2010.
16. Baude, P. F. and S. D. Theiss, "RFID sensor," US 2007/0215709 A1, Sep. 2007.
17. Marinov, V. R., Y. A. Atanasov, A. Khan, D. Vaselaar, A. Halvorsen, D. L. Schulz, and D. B. Chrisey, "Direct-write vapor sensors on FR4 plastic substrates," *IEEE Sensors Journal*, Vol. 7, No. 6, 937–944, Jun. 2007.
18. Loo, C.-H., K. Elmahgoub, F. Yang, A. Elsherbeni, D. Kajfez, A. Kishk, and T. Elsherbeni, "Chip impedance matching for UHF RFID tag antenna design," *Progress In Electromagnetics Research*, Vol. 81, 359–370, 2008.
19. Rao, K. V. S., P. V. Nikitin, and S. P. Lam, "Impedance matching concepts in RFID transponder design," *Fourth IEEE Workshop on Automatic Identification Advanced Technologies (AutoID'5)*, 39–42, 2005.
20. Griffin, J. D., G. D. Durgin, A. Haldi, and B. Kippelen, "RF tag antenna performance on various materials using radio link budgets," *IEEE Antennas and Wireless Propagation Letters*, Vol. 5, 247–250, 2006.
21. Griffin, J. D., "A radio assay for the study of radio frequency tag antenna performance," Master's Thesis, Georgia Institute of Technology, Atlanta, 2005.
22. Lázaro, A., D. Girbau, and D. Salinas, "Radio link budgets for UHF RFID on multipath environments," *IEEE Trans. Antennas Propagat.*, Vol. 57, No. 4, 1241–1251, Apr. 2009.
23. Standard dipole, [Online] Available: http://www.testmart.com/sp.cfm/ANT/ANRI/MP651B.html.
24. CST-Microwave Studio, *User's Manual,* 2006.
25. NXP UCODE G2XL, Ultrahigh frequency smart label ICs [Online] Available: http://www.nxp.com/acrobat_download/literature/9397/75016225.pdf.
26. Light weight concrete, [Online] Available:http://www.ebrindia.com/cellular-light-weight-concrete-blocks.htm.
27. Smart block [Online] Available: http://www.smartblock.in.th/view_product.php?product=A001&mcat=&cat_id=137&lang=th&page=1.
28. Stavrou, S. and S. R. Saunders, "Review of constitutive parameters of building materials," *2003 Antennas and Propagation (ICAP 2003)*, 211–215, Apr. 2003.

29. Takizawa, T., "Reduction of ghost signal by use of magnetic absorbing material on walls," *IEEE Trans. on Broadcasting*, Vol. 25, No. 4, 143–146, Dec. 1979.
30. Jin, X. and M. Ali, "Embedded antennas in dry and saturated concrete for application in wireless sensors," *Progress In Electromagnetics Research*, 197–211, 2010.
31. Jin, X. and M. Ali, "Reflection and transmission properties of embedded dipoles and PIFAs inside concrete at 915 MHz," *2009 IEEE Antennas and Propagation Society International Symposium, APSURSI' 09*, 1–4, Jun. 2009.
32. Hasar, U. C., "Permittivity determination of fresh cement-based materials by an open-ended waveguide probe using amplitude-only measurements," *Progress In Electromagnetics Research*, Vol. 97, 27–43, 2009.
33. Dielectric probe, [Online] Available: http://www.home.agilent.com/agilent/product. jspx?pn=85070E&lc=eng&cc=US.
34. Lee, J. W. and B. Lee, "Design of high-Q UHF radio-frequency identification tag antennas for an increased read range," *IET Microw. Antennas Propagat.*, Vol. 2, No. 7, 711–717, Apr. 2008.
35. Nakhla, N., A. A. El-deen, K. Maurice, L. Youssef, N. Mahfouz, T. Youakim, M. N. A. Zeid, K. Nassar, and A. Darwish, "Electrostatics utilization for concrete performance measurements," *2010 IEEE Middle East Conference on Antennas and Propagation (MECAP 2010)*, 1–2, Oct. 2010.
36. Ford, S. J., J.-H. Hwang, I. D. Shane, R.A. Olson, G. M. Moss, H. M. Jennings, and T. O. Mason, "Dielectric amplification in cement pastes," *Advanced Cement Based Materials*, Vol. 5, No. 2, 41–48, Mar. 1997.
37. Wen, S. and D. D. L. Chung, "Cement-based materials for stress sensing by dielectric measurement," *Cement and Concrete Research*, Vol. 32, No. 9, 1429–1433, Sep. 2002.